Geophys. J. Int. (2006) **165,** 383–398 doi: 10.1111/j.1365-246X.2006.02867.x

Lithospheric and upper mantle structure of central Chile and Argentina

Hersh Gilbert, Susan Beck and George Zandt

University of Arizona, Department of Geosciences, 1040 *East Fourth Street, Tucson, Arizona,* 85721*, USA. E-mail: hgilbert@geo.arizona.edu*

Accepted 2005 November 7. Received 2005 September 9; in original form 2005 February 24

SUMMARY

The tectonics of central Chile and Argentina have been greatly affected by the shallow dips of the subducting Nazca plate, which controlled patterns of magmatism and deformation nearly 1000 km away from the plate boundary. We calculate receiver functions from data recorded by the CHARGE array, which transected the Andes and Sierras Pampeanas in central Chile and Argentina, to better constrain the crustal structure of this region. Beneath the northern transect of the CHARGE array, where the Nazca slab flattens near 100 km, we find the crust is over 60 km thick beneath the Andes and thin to the east. The thick crust, however, extends ∼200 km to the east of the high elevations. Estimates of V_P/V_S obtained from receiver functions vary along ancient terrane boundaries exhibiting higher values to the west. Interestingly, we observe that the amplitude of the phase corresponding to the Moho on receiver functions diminishes to the west, complicating our images of crustal structure. We proposed that the observations presented here of thickened crust within a region of low elevations, diminished receiver function arrivals, and reports of high shear-wave speeds atop of the mantle wedge overlying the shallowly subducted Nazca slab, can be explained by partial eclogitization of the lower crust. The Moho appears simpler across the southern transect where it can be identified near 50 km depth at its deepest point beneath the Andes and shallows eastwards. Volcanism remains active near the latitudes of our southern transect and we observe multiple crustal low-velocity zones indicative of regions of partial melt near the centres of volcanism. Signals related to the Nazca slab remain more elusive, suggestive of a small impedance contrast between the slab and overlying mantle.

Key words: Andes, crustal structure, flat subduction, lithospheric deformation, Sierras Pampeanas, receiver functions.

INTRODUCTION

The occurrence of continental deformation several hundreds to over 1000 km away from plate boundaries has been attributed to forces associated with shallow subduction (e.g. Bird 1984). Currently flat slabs exist in several places on the Earth and comprise 10 per cent of subduction zones worldwide (van Hunen *et al.* 2002), yet few detailed images of shallow subduction exist. The causes of shallow subduction are still not fully understood (see van Hunen *et al.* 2002, and references therein). Some insight into factors responsible for flat subduction can be gained from the recognition that locations of the largest flat slab segments occur beneath the fastest overriding plate motion (Jarrard 1986) suggesting that high convergence rate plays a role, additionally locations of subducting oceanic plateaus correlate with sites of shallow flat subduction (Gutscher *et al.* 2000; Yañez *et al.* 2002) indicating that plateaus may also play an important role. However, better knowledge of the structure of the slab, overriding crust, and mantle wedge above the flat slab will provide much needed information to advance our understanding of how the overriding lithosphere is affected by the flat slab.

One often-sited example of the effects of shallow subduction has been the pervasive deformation within the western United States that has been attributed to flat subduction during the Laramide. The Sierras Pampeanas, consisting of thick-skinned basement-cored uplifts to the east of the Andes, is another region that has undergone deformation well away from a plate boundary and may have been driven by the flattening of the Nazca slab during the last 5–7 Ma (e.g. Kay *et al.* 1991; Ramos *et al.* 2002). The southern Andes north of 33.5°S are characterized by a lack of arc magmatism along the Precordillera and is thought to be underlain by a segment where the Nazca slab shallowly subducts between latitudes ∼28° and 32°S (Cahill & Isacks 1992; Ramos *et al.* 1996) (Fig. 1). A narrow belt of eastward migrating, thin-skinned, Neogene to Quaternary shortening has affected the Andes themselves (Jordan *et al.* 1983). Further to the east, the Pampean ranges consist of crystalline basement uplifted on reverse faults during the Plio-Pleistocene (Jordan *et al.* 1983).

The southern extent of the Precordillera fold-and-thrust belt coincides with the transition between flat subduction to the north and steeper subduction to the south at 33.5°S. The extent of the

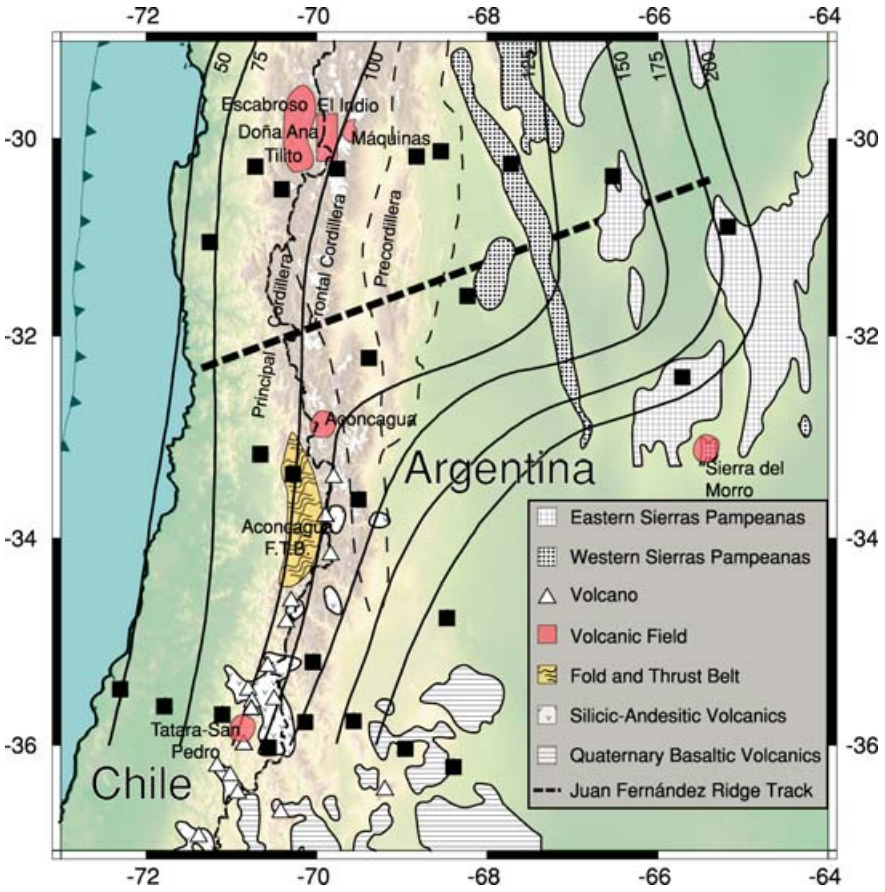

Figure 1. Map of volcanism discussed in the text including the Sierra del Morro, Doña Ana, and Máquinas areas as well as other important landmarks such as the Aconcagua region. The track of the Juan Fernández Ridge is shown as a heavy dashed line and solid lines mark the depth contours of the Nazca slab (Cahill & Isacks 1992). Thin dashed lines mark the boundaries between the Principal Cordillera, Frontal Cordillera and Precordillera. Locations of various volcanic fields noted in legend after Jordan *et al.* (1983) are shown for reference.

fold-and-thrust belt appears to be controlled by an Early Ordovician carbonate platform that continues several hundreds of meters further south, indicating that the truncation of the Precordillera is not related to a palaeogeographic change (Ramos *et al.* 2002). However, other work has emphasized the importance of palaeogeology on the tectonic style of the forelands further north (Allmendinger *et al.* 1983; Cahill & Isacks 1992; Grier *et al.* 1992). The geological differences between provinces have been found to coincide with differing upper mantle structures (Whitman *et al.* 1992), suggesting that mantle structure and consequential rheological differences of the foreland lithosphere also contributes to the variations in the style of foreland deformation. Within the crust, it is evident that the depth to the brittle–ductile transition beneath the Andes appears to be correlated with magmatic activity and the location of crustal wedges in the thrust front of the Sierras Pampeanas (Kay *et al.* 1991).

While it is widely recognized that the Sierras Pampeanas region of South America is a collage of accreted terranes (e.g. Ramos *et al.* 2002) no consensus has been reached regarding the structural outline of basement terranes in the western region of Argentina and the timing of the various collisions. The boundaries between terranes have strongly influenced younger tectonic events as studies have shown that shear zones formed during ancient collisional events were reactivated during Cenozoic faulting (e.g. Schmidt *et al.* 1994). Precambrian structural fabrics within ductile shear zones control the western vergence of those Andean brittle faults (Ramos *et al.* 2002). A major suture has been recognized between the Laurentia-derived Cuyania terrane and Famatina terrane on the basis of lithologic differences, gravity and magnetic anomalies, sedimentary and volcanic history, and reprocessing of deep seismic industrial reflection lines (Zapata & Allmendinger 1996). Another major suture is located along the eastern side of the Sierra de Famatina, where mafic Ordovician rocks are exposed and have been interpreted as the major suture between the Famatina and Pampia terranes, which are thought to be associated with important mylonitic shear zones formed during the Early Palaeozoic (Ramos *et al.* 2002). A third important suture, on the eastern side of the Pampia terrane between it and the Rio de La Plata craton (Fig. 2) coincides with Cenozoic Andean faults. The collisional episodes that occurred during the Late Proterozoic and Early Palaeozoic times in this part of southern South America resulted in deformation within the basement expressed by schistosity and foliation with the growth of discrete ductile shear zones (Ramos *et al.* 2002). Nearly 200 km of crustal shortening along thrust belts following the Oligocene further contributed to the present day tectonic setting across the flat slab region (Allmendinger *et al.* 1990). The temporal correlation between periods of crustal thickening and shortening illustrates that much of crustal thickening resulted from shortening (Kay & Abruzzi 1996).

At ∼20 Ma the tectonic setting of the Precordillera had not yet been affected by the collision of the Juan Fernandez Ridge (Fig. 1). Volcanism was present in the High Cordillera at the latitudes of

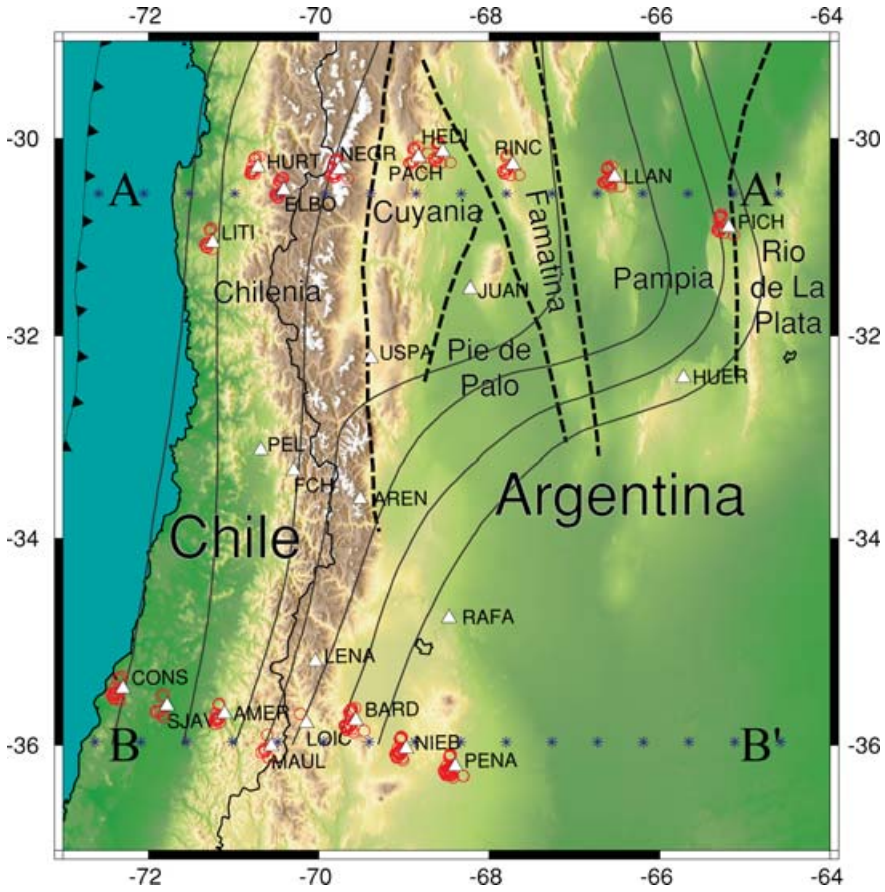

Figure 2. Map of topography and the PASSCAL broad-band seismic stations in central Chile and Argentina that comprise the CHARGE array used in this study (white triangles). Piercing points of P_ds waves, which fan out away from each station with increasing depth, are shown as red circles. Points presented here correspond to P_ds waves at 50 km depth. CCP bin locations are shown as asterisks spaced at 60 km. Solid lines denote depth contours of the subducted Nazca slab from Cahill & Isacks (1992). Dashed lines mark locations of suture zones from Ramos *et al.* (2002) between the Cuyania, Pie do Palo, Famatina, and Pampia terranes, and the Rio de La Plata craton.

flat subduction until ∼11 Ma at which time it began to migrate eastwards nearly 500 km until shutting off around 5 Ma (Kay *et al.* 1987, 1988). The first migration of the volcanic arc eastwards towards the Sierras Pampeanas is recorded in the volcanics of the Aconcagua region (Fig. 1). The shifting of magmatism followed a short period of deformation in the western half of the Aconcagua fold and thrust belt (Ramos *et al.* 1996). Huge amounts of andesitic and dacitic rocks were erupted at approximately 16 and 9 Ma in the Aconcagua massif. This pattern of volcanism has been interpreted to result from the gradual flattening of the slab over time (see Kay & Mpodozis 2002, and references therein). Arc magmatism returns further south where the slab returns to a more normal dip of 30°. Changes in the amount, location, and composition of volcanism over the last 25 Ma have provided petrologic evidence for the slab flattening (e.g. Kay *et al.* 1991). The changes in volcanism over time have included a decrease in the rate of volcanic activity culminating in a distinct lack of Quaternary volcanism above the flat slab segment between 28° to 33°S (Jordan *et al.* 1983; Kay & Mpodozis 2001, 2002; Ramos *et al.* 2002). The only magmatism in the region in the Pliocene is restricted to the eastern part of the Sierras Pampeanas before the final extinction of volcanism in the flat-slab segment at the Sierra del Morro (1.9 Ma) (Ramos *et al.* 2002). The range in composition of volcanic activity narrowed while its rate decreased, contemporaneously its average silica content increased and it appeared to originate from a more garnet-rich source region (Kay *et al.* 1987). Both of these trends have been interpreted to be associated with the thinning of the underlying wedge of asthenospheric mantle and formation of garnet in the thickened crust (Kay *et al.* 1987).

Investigations into crustal structure of this region based on geophysical (e.g. Allmendinger *et al.* 1990; Introcaso *et al.* 1992; Regnier *et al.* 1994; Gimenez *et al.* 2000; Fromm *et al.* 2004; Alvarado *et al.* 2005) and geochemical observations (e.g. Kay *et al.* 1987) have found evidence for thick crust beneath the High Cordillera. Patterns of the evolution of crustal thickness as inferred from trends in mineralization ages indicate a southward progression of crustal thickening that correlates with the southward younging in mineralization (Kay *et al.* 1991). A detailed analysis of *Pn* arrivals within this region illustrate the existence of extensive regions of thickened crust that are over 50 km thick well beyond the region of high elevations within the Andes (Fromm *et al.* 2004). Isostatic considerations point to the need for significant lateral variations in the source of buoyancy to reconcile the presence of thick crust and low elevations juxtaposed to regions of similarly low elevations and thin crust to the east and substantially higher elevations and similarly thick crust to the west. Either variations in the buoyancy contribution from the mantle or density variations in the crust could provide mechanisms by which to reconcile this observed paradox.

We investigate variations in crustal and upper mantle structure across Chile and Argentina through the use of common conversion point (CCP) stacking of teleseismic receiver functions calculated from data recorded by the CHARGE array. The Chile Argentina Geophysical Experiment (CHARGE) was a PASSCAL array composed of 22 broad-band portable seismometers. These instruments were mostly deployed in two east–west transects across Chile and Argentina near 30°S and 36°S for 18 months between 2000 November and 2002 May. The average spacing between stations was near 70 km permitting us to investigate general trends in crustal and upper mantle structure across an extended distance.

DATA AND METHOD

Our analysis used recordings from teleseismic *P* and *PP* phases to calculate receiver functions that isolate receiver side *P*- to *S*-wave conversions. Receiver functions are sensitive to sharp changes (discontinuities) in shear wave speeds and have been widely used in the past for studying the crust and upper mantle (e.g. Phinney 1964; Langston 1977; Owens *et al.* 1984). Here we employ a geographic stacking scheme that helps to identify variations in structure and benefits from utilizing multiple stations that sample the same geographic region and continuous features become apparent while signal generated noise stacks incoherently (Clouser & Langston 1995). This method of stacking also helps in determining the lateral extent of features.

We used 50 teleseismic events (for *P* and *PP* phases) recorded by the array to generate CCP receiver function cross-sections migrated to depth (e.g. Dueker & Sheehan 1997; Li *et al.* 1998; Gilbert & Sheehan 2004). Stacking together many receiver functions that sample the same subsurface area dramatically improves signal to noise and small amplitude features can be resolved. These techniques have led to high-resolution images of mantle discontinuity topography (Dueker & Sheehan 1997; Li *et al.* 1998) and crustal structure (Wilson *et al.* 2003; Zandt *et al.* 2004). We geographically stack receiver functions calculated from data recorded by the CHARGE experiment in common conversion bins (Fig. 2), which take advantage of the lateral coherence between receivers to produce reflection-style images of crust and mantle structure over a variety of scales rather than spot estimates. Over 340 receiver functions were used in this study. The source-receiver separation for *P* waves used range from 30° to 95°, where rays bottom in the lower mantle, while events producing *PP* phases that could be used for receiver function calculation occurred within the 88° to 171° distance range. Only events with good signal-to-noise ratios and with strong radial *P* or *PP* waves that can be seen after deconvolution were utilized in our analysis.

The earthquakes used are located mainly at western (southwestern Pacific) and northwestern (central America) backazimuths relative to the CHARGE array. The dearth of seismicity at teleseismic distances to the east of the CHARGE array prevents sampling structures from a complete range of azimuths. Specifically, we found only a single event in the eastern hemisphere of backazimuthal range, and it was not well recorded by our entire array. We, therefore, are hindered in our ability to utilize receiver function techniques that rely upon investigating phases as a function of azimuth. Investigations into the azimuthally dependant effects of dipping layers on receiver function arrivals have shown that for an eastward-dipping layer, waves incident from western azimuths produce the smallest amplitude converted phases (Owens *et al.* 1988). Our ability to image the eastward-dipping portion of the slab with events from western backazimuths will be hindered by this effect. However, this should not affect our ability to image the flat slab as it would appear similarly when sampled from any direction.

In this study, receiver functions are calculated for seismograms with clear *P*- or *PP*-wave arrivals on both the vertical and radial components, by deconvolving the vertical from the radial seismogram. The deconvolution is accomplished through an iterative approach that relies on the cross-correlation of the vertical and radial seismic records (Ligorria & Ammon 1999). The variance reduction of the calculated receiver function is found after each iteration to determine the quality of the deconvolution. The iterations continue until one of two criteria is met; either the improvement in variance reduction falls below a predetermined level, or the number of iterations reaches its maximum limit. Receiver functions are then analysed for each station individually, and stacked together with others from nearby stations. We geographically bin the ray set and perform CCP stacks of receiver functions. Paths of *P* waves and converted *S* waves are traced through a grid of bin points with a constant V_P of 6.2 km s^{-1} and V_P/V_S of 1.75 down to 70 km depth to migrate features within the crust. It is unlikely that crustal thicknesses reach 70 km, yet this depth is chosen to insure that crustal features are not artificially mapped too deep by mistakenly migrating them with mantle velocities. At greater depths V_P increases to 7.8 km s^{-1} to migrate mantle structures. As discussed below, lateral variations in V_P/V_S are identified across the CHARGE array. Accounting for these variations would affect our greatest crustal thicknesses by less than 10 km and not significantly modify the general crustal structure. Piercing points are found at each 1 km depth interval. A grid of bin points is constructed, spaced 50 km apart. Each bin has a radius of 75 km, resulting in sharing between adjacent bins (Fig. 2).

OBSERVATIONS

Individual stations display distinct differences in the character of receiver functions recorded in differing tectonic settings, and within tectonic settings. Across the northern transect, where different terranes are sampled, differences in receiver functions appear to coincide with major sutures between the Cuyania, Famatina, and Pampia terranes. Where the southern transect crosses the high Andes and active volcanism is present, we observe large negative arrivals that can result from the presence of crustal low-velocity zones. Crustal low-velocity zones in a region with active volcanism could indicate the location of crustal magma chambers. An observation common to both the northern and southern transects is the strong Moho signal in the tectonically stable eastern portion and significantly reduced Moho signal to the actively deforming west. To convey the extreme variability of the CHARGE data set, we present individual, unstacked receiver functions from a sample of stations that contain traces representative of each region.

The station HEDI, in the transition between the Precordillera and the western Sierras Pampeanas (Fig. 2), exhibits large negative arrivals following the *P* wave in many of the receiver functions as well as a positive arrival prior to 2.5 s and between 4 and 5 s (Fig. 3a). The source of this negative arrival is somewhat ambiguous as there is no recent volcanism in this area and therefore, we do not expect to find zones of partial melt, and their associated low-velocity zones. At later times corresponding to greater depths, it is difficult to identify any coherent arrivals that span across all backazimuths. A similar lack of coherent signal near the expected arrival time of the Moho phase is observed at other stations (e.g. JUAN, USPA and RINC) in both the Cuyania and Famatina terranes (Figs 3b–d). There are,

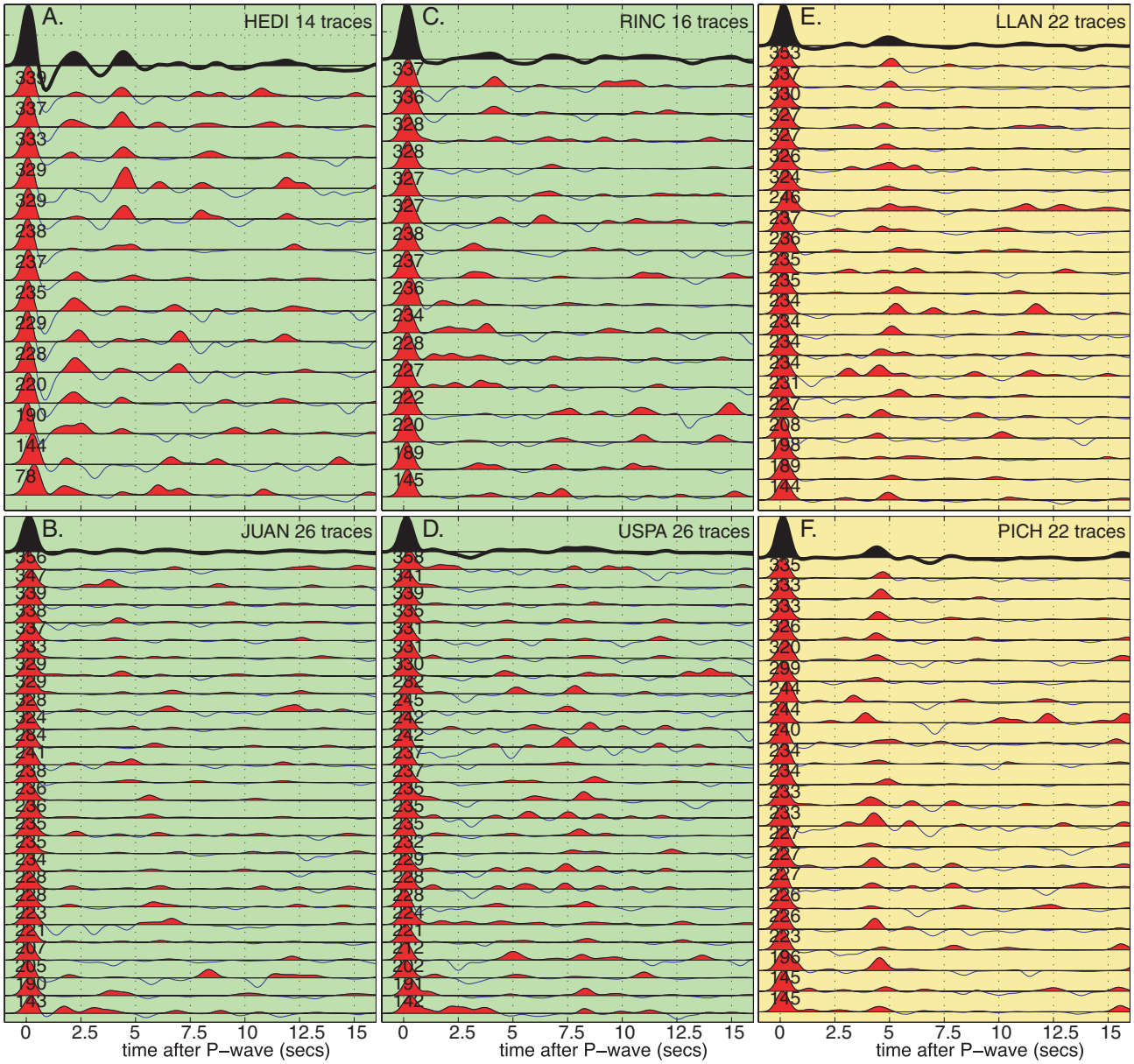

Figure 3. Unstacked receiver functions plotted as a function of time for stations HEDI (a), JUAN (b), RINC (c), USPA (d), LLAN (e) and PICH (f) in the northern portion of the CHARGE array. Traces for each station are sorted by backazimuth, which is noted on the left edge of individual traces near the *P*-wave arrival. Positive amplitudes are filled red. The average of all the receiver functions for each station is plotted and filled in black at the top of each panel. Phases corresponding to the Moho can be identified near 5 s for stations LLAN and PICH while other stations do not display arrivals that appear coherent on multiple traces.

however, arrivals present on receiver functions recorded within the Cuyania terrane that appear to coincide with fault bounded crustal layers that have been inferred to be in the 20 and 35 km depth range (Ramos *et al.* 2002). At stations USPA and JUAN within the Cuyania terrane, arrivals are present around 5 and 8 s after the *P* wave corresponding to depths between 40 and 65 km. Although these arrivals are present, they are not clearly detected on all traces. The arrival may have an azimuthal dependence as it appears weakest from northern and southern azimuths.

The receiver functions from both PICH and LLAN, which are in the Pampia terrane, are remarkably simpler than those from stations on either the Cuyania or Famatina terranes (Figs 3e and f). On both of these stations, the Moho arrival can be clearly found close to 5 s after the *P* wave. The presence of a clear Moho arrival is indicative of a significant velocity contrast between the crust and mantle, similar to that found across the Moho in many continental regions. The Moho signal at these stations is clearly the most prominent and azimuthally consistent arrival. At PICH the Moho arrivals appear slightly earlier than at LLAN, indicative of a thinner crust beneath PICH than LLAN, which agrees well with our receiver function cross-sections presented below. Stations to the west display significant variations as a function of azimuth. This characteristic no longer holds to the east where receiver functions at PICH and LLAN do not appear as strongly dependant on azimuth.

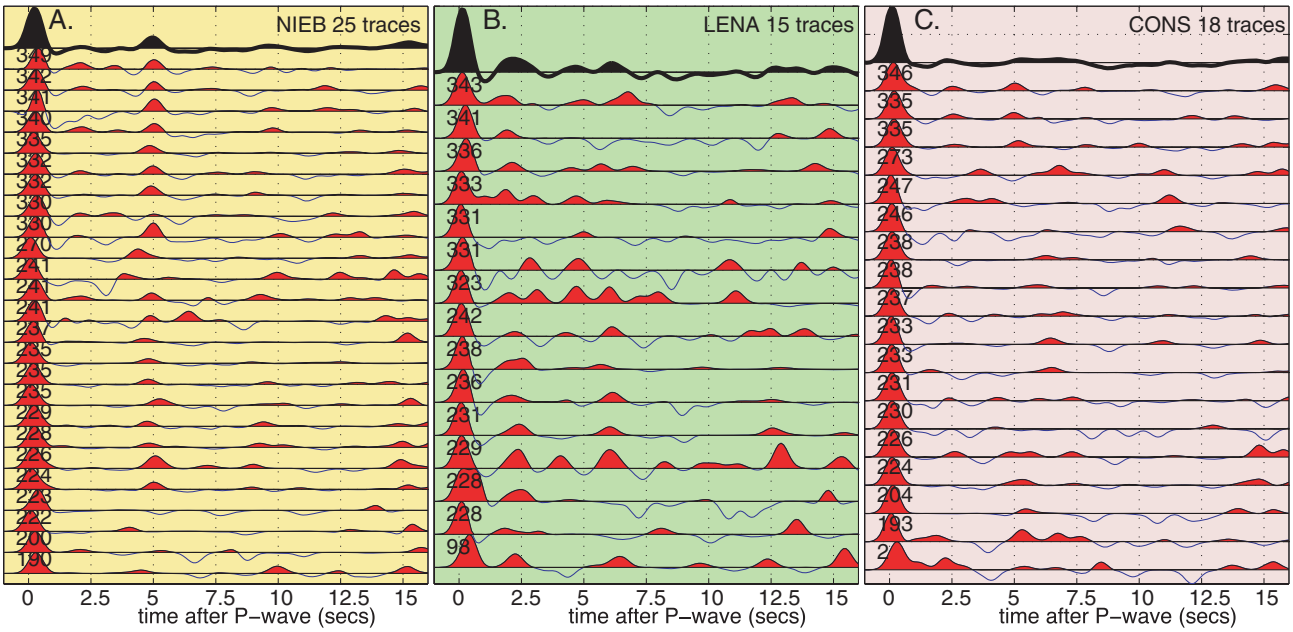

Figure 4. Same as Fig. 3 except for stations NIEB (a), LENA (b) and CONS (c) within the southern portion of the CHARGE array. Similarly, clear Moho signal can only be found on NIEB.

The Moho signal in the eastern portion of the southern transect appears similar to that of the eastern portion of the northern transect. Station NIEB, is one example of a station in the east that displays a strong coherent Moho signal (Fig. 4a). Stations BARD and PENA, which are similarly located in the eastern portion of the southern transect also display a strong Moho signal as can be seen from the prominent arrival in the stacked cross-section. As in the northern transect, the Moho signal diminishes to the west as the southern transect crosses the higher elevations in the Andes. Receiver functions at station LENA in the Andes also exhibit a negative arrival directly after the *P* arrival that is followed by a periodic ringy signal (Fig. 4b). Strong positive arrivals can be seen close to 2 and 6 s after the *P* wave in many of the traces. Further west, receiver functions from station CONS in the forearc of the southern transect does not exhibit strong coherent arrivals that can be detected from multiple traces (Fig. 4c).

East–west cross-sections of CCP stacks are presented in Figs 5(a) and (b). The prominent positive arrivals in the 30–60 km depth range correspond to the Moho arrival and illustrate variations in crustal thickness. These cross-sections illustrate the ∼30 km of variation in crustal thickness across the region as well as the profound degree of variability in crustal structure and Moho signature. To compare crustal structure and physiographic provinces, surface topography along the cross-sections is plotted above each profile. Mid-crustal features can also be found on these cross-sections, but in some areas have smaller amplitudes. The mid-crustal arrivals observed here are generally less laterally coherent than the Moho arrival. A mid-crustal arrival can be seen between longitudes 71° and 65.5°W on the northern cross-section and 72° and 70°W on the southern.

Regional trends in crustal structure can be found by constructing a map of crustal thickness (Fig. 6a) combining CHARGE observations with past observations from the PANDA array (Regnier *et al.* 1994) and off-shore refraction data (Flueh *et al.* 1998) within this region. Clearly the creation of such a map entails interpolating measurements over distances of hundreds of kilometres, but still illustrates significant findings. The thick crust present in the western Sierras Pampeanas persists south of the northern transect as we find thick crust of over 50 km thick at the station JUAN, many of the PANDA stations, and the thickest crust at the station USPA (Fig. 6b), that reaches 64 km thick. The thinner crust and simpler Moho signal of the craton that is present at LLAN and PICH continues south to HUER, and exhibits similar characteristics to that in the backarc of the southern line. Thin crust of less than 30 km thick is present along the west coast of South America as observed at the stations in the western portion of the northern CHARGE transect and the off-shore lines (Fig. 6a). The thick crust in the northern portion of our study area extents well to the east of the Cordillera into the western Sierras Pampeanas, and roughly overlies the region of flat subduction (Fig. 6a). Inspection of stacked receiver functions from stations south of the northern transect indicate that the mid-crustal arrivals present on the northern transect continue southwards to at least USPA and JUAN (Fig. 6b). South of USPA, mid-crustal arrivals are also present at AREN, but any relation between arrivals observed at AREN and those further north remains speculative.

Northern transect

Our stacked images for the northern array of stations display a great deal of variability in crustal structure. The receiver function arrivals from the Moho change in character from west to east, possessing low amplitude weak arrivals to the west while appearing stronger further east. Based on these arrivals, the crust below the Andes in the central portion of the northern cross-section is greater than 60 km thick. Further east, the crust thins, but much more gradually than the surface elevations decrease in such a manner that thick crust underlies the lower elevations of the western Sierras Pampeanas with average elevations near 1 km. Due to the low amplitude arrivals from the Moho in the western portion of our study area, we corroborated our receiver function observations with the *Pn* analysis of Fromm

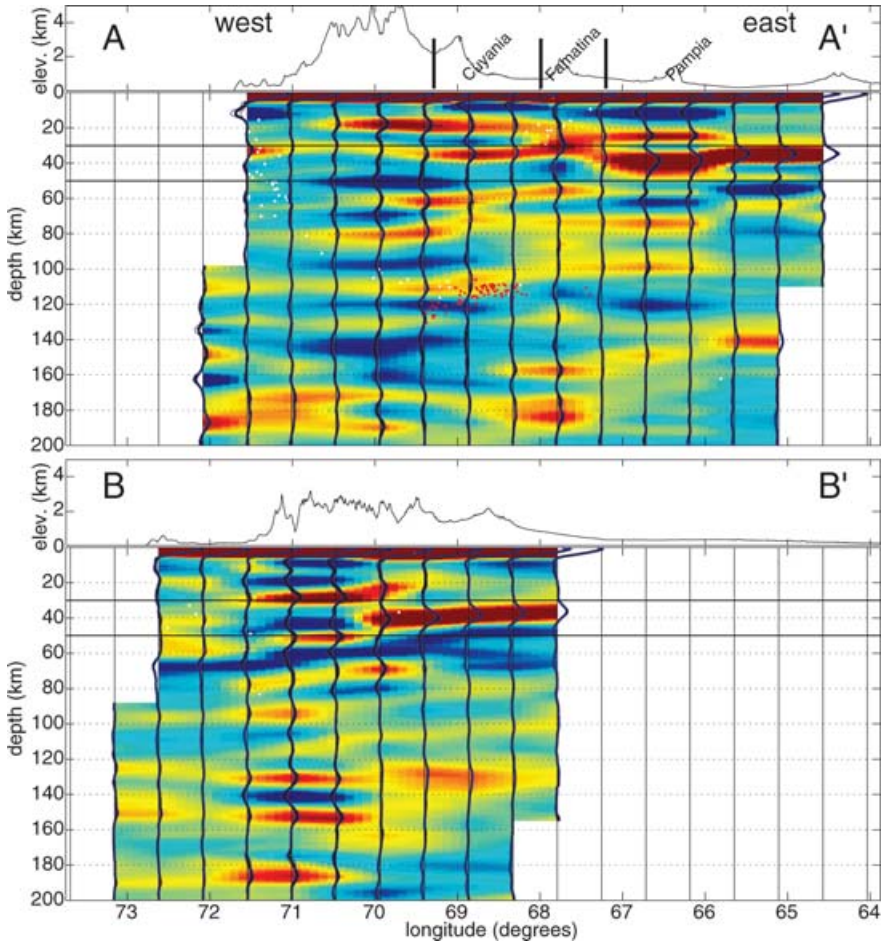

Figure 5. West to east cross-sections of CCP stacked receiver functions for the northern (a) and southern (b) CHARGE transects. Locations of cross-sections are presented on Fig. 2 (A-A′ and B-B′). Positive arrivals are shown as red while negative appear as blue. Stacked receiver functions for each column of CCP bins are shown in black along with their one-sigma bounds derived from bootstrap resampling. Horizontal lines are drawn at 30 and 50 km depth for reference. Clear, simple Moho arrivals can be seen as the large red arrival, near 40 km depth in the eastern portion of each cross-section. Cross-sections of surface topography, along with terrane boundaries are presented above each stacked image. In order to aid in identifying the location of the slab earthquake locations from Engdahl *et al.* (1998) (white dots) along with seismicity relocated with the CHARGE array (red dots) have been plotted on the cross-sections. Note the near horizontal pattern of seismicity close to 100 km depth on the northern cross-section between longitudes 70°W and 68°W.

et al. (2004) to verify that the arrivals were indeed due to the Moho (Fig. 7a).

The crust below the Andes appears to reach its greatest thickness along the northern transect of 63 km at a longitude near 70°W, which closely corresponds to the longitude of the high Andean peaks that reach altitudes close to 4.5 km at this latitude (Fig. 5a). Other arrivals, which mark intercrustal structures, are also present within the western crust at depths near 20 and 40 km. The clearly observed mid-crustal arrivals present below the high Andes continue further east below the western Sierras Pampeans. The changes in intercrustal structure appear to correlate with, and may relate to, ancient terrane boundaries. Differences observed in the impedance contrast across the Moho coincide with locations of the boundaries between the Cuyania, Famatina, and Pampia terranes presented by Ramos *et al.* (2002). The observed boundary between the clear Moho signal in the east and the more complex signal to the west is close to the terrane boundary between the Famatina and Pampia terranes.

By comparing arrival times of direct and multiple phases on receiver functions (Zandt *et al.* 1995) we determine that the crustal V_P/V_S ratio varies across the northern transect with lower values near 1.75 to the east of 67°W, indicative of felsic crust, and higher values over 1.8 to the west, that can result from a more mafic crust (Fig. 7a). Other changes in lithology can also contribute to average crustal V_P/V_S variability such as eclogitized lower crust. Differences in crustal V_P/V_S across the northern transect agree with expectations based on compositions of the terranes that comprise the crust that have been found to be more mafic in the western Sierras Pampeanas (e.g. Ramos *et al.* 2002).

Southern transect

Along the southern transect, clear converted phases from the Moho appear east of the Andes (∼70.5°W Fig. 5b) in Argentina and extend to the eastern edge of our study area near 68°W. To the west of 70.5°W, the crust increases in thickness and complexity, the single Moho arrival appears to bifurcate into two separate arrivals, one shallower than the Moho signal to the east at ∼30 km depth, and a second deeper arrival close to ∼50 km depth (Fig. 5b). This pattern of multiple positive arrivals is indicative of multiple abrupt increases in seismic velocities, a configuration that could result from a

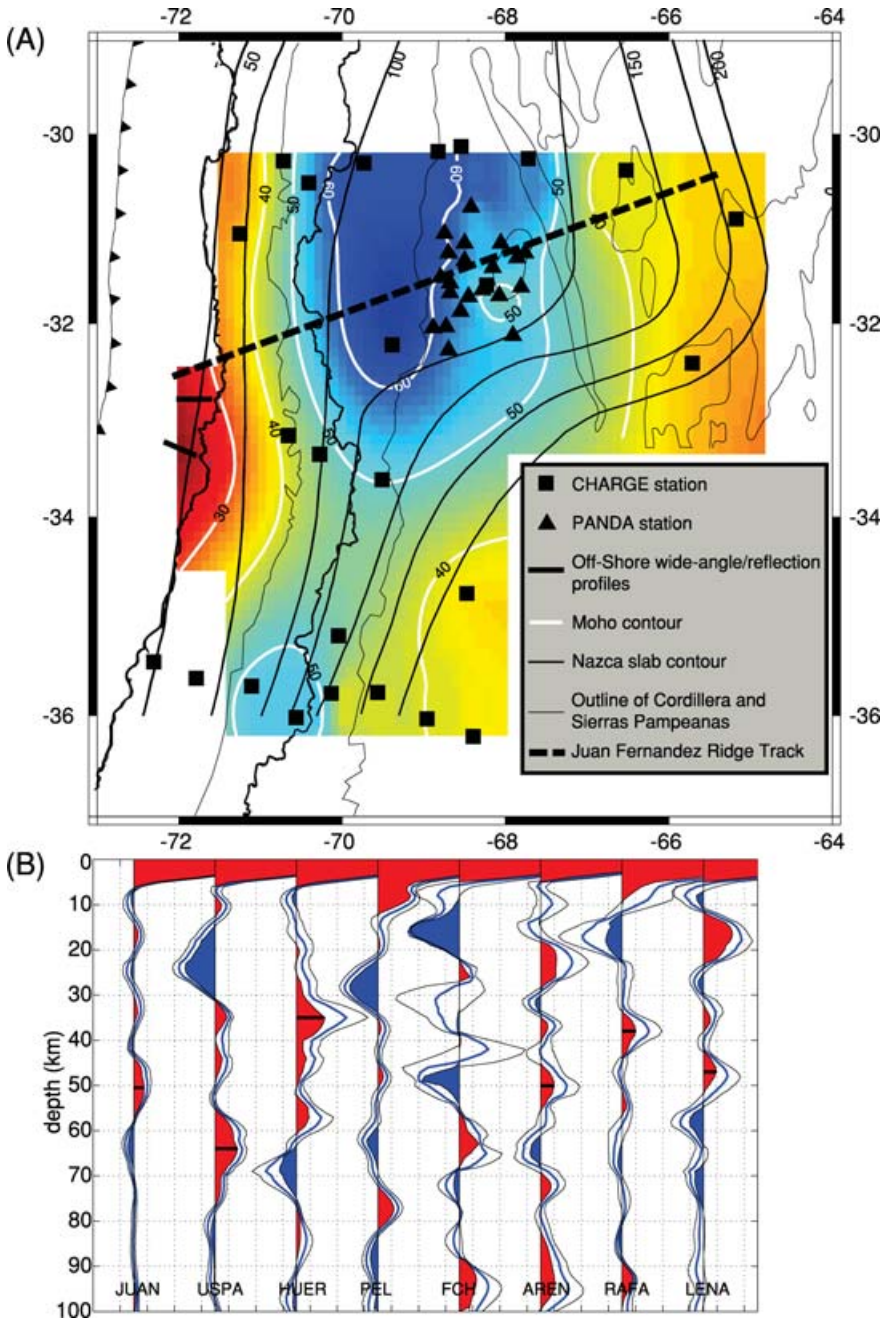

Figure 6. (a) Colour contour map of crustal thickness. Regions of thicker crust, which reach up to 64 km thick, are shown in blue, while areas of thinner crust, which thins to as little as 25 km, are shown in red. Locations of CHARGE stations are shown as black squares, PANDA stations (Regnier *et al.* 1994) as black triangles, and off-shore profiles (Flueh *et al.* 1998) as thick black lines. Also note locations of slab contours (black lines) of Cahill & Isacks (1992) and outlines of ranges (thin black lines). (b) Stacked receiver functions from stations between northern and southern transects that contributed to the crustal thickness map. Thick black lines indicate crustal thicknesses that could be picked, which were used to create the Moho map.

differentiated crustal composition with a high-speed lower crust underlying a lower-speed upper crust. The crustal V_P/V_S ratio is greater than 1.8 across the entire extent of the southern transect (Fig. 7b). Differently from the western portion of the northern transect where high V_P/V_S appears to be related to compositional effects, the source of high V_P/V_S could relate to the presence of partial melt, which is likely to be present near active volcanic centres. The continuation of high V_P/V_S further to the east into the back arc likely marks the presence of magma related to the extensive backarc volcanism present in this area (Jordan *et al.* 1983). Interestingly large negative receiver function arrivals are not present at mid-crustal levels in this region, suggesting a smaller amount of molten material than further west where large negatives are present.

Large negative arrivals near 20 and 40 km depth occur above both of the positive arrivals, between longitudes 70.5°W and ∼71.5°W, and coincide with the locations of recent volcanism (Fig. 5b). It is

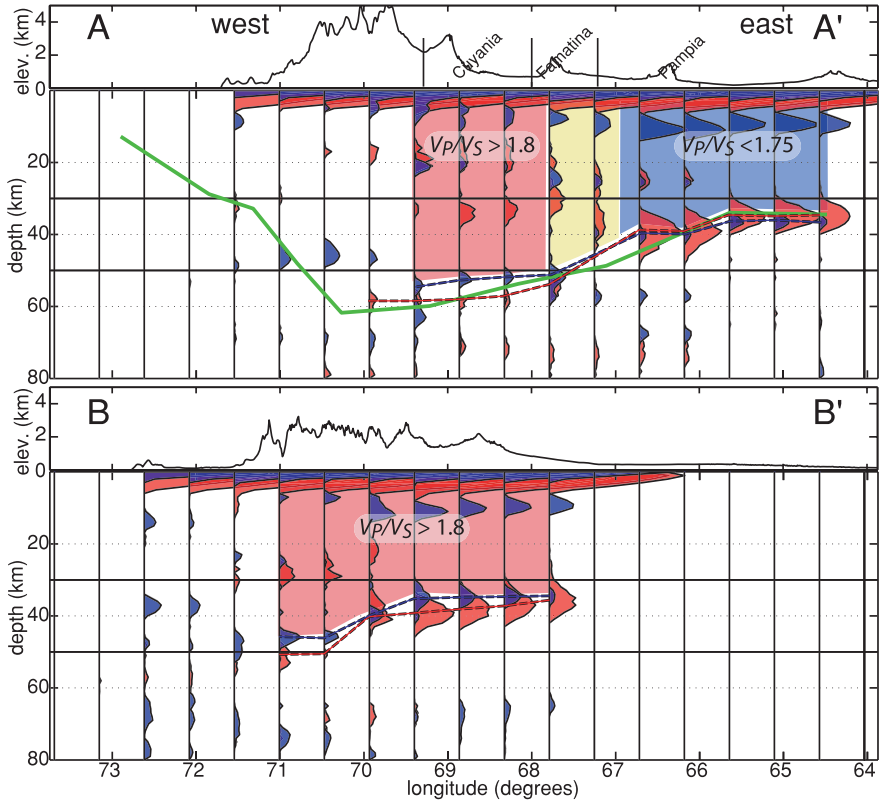

Figure 7. West-to-east stacked receiver function cross-sections comparing crustal thicknesses derived from P_ds (solid red line) and P_PP_ds (solid blue line) phases used to calculate crustal V_P/V_S ratios for the northern (A) and southern (B) CHARGE transects. Regions with deeper P_ds picks than P_PP_ds possess V_P/V_S values that are higher than the value of 1.75 used to migrate from time to depth while creating stacks. Overlain are solid colours illustrating general trends in V_P/V_S values found in this study (red-high V_P/V_S; blue-low V_P/V_S) as well as crustal thickness estimates derived from *Pn* arrivals displayed as a green line along the northern transect (Fromm *et al.* 2004).

likely that these negative arrivals result from low seismic velocities associated with magmatism and volcanism (Hildreth & Moorbath 1988; Feeley *et al.* 1998; Costa *et al.* 2002). Interpreting each of these arrivals can be complicated because the later phase could actually be a reverberation within the low-velocity zone. Commonly, moveout analysis, where the arrival times of phases are investigated as a function of ray parameter, is used to determine if an arrival results from a reverberation or not, but cannot be employed here due to limited ray parameter sampling. The observations we have are consistent with multiple direct arrivals.

At subcrustal levels in the mantle wedge there is a large continuous negative arrival that follows the base of the crust increasing in depth as crustal thickness increases. This continuous negative arrival may result from multiple factors across the profile as inferred in part from negative arrivals crossing the location of the subducting slab, which is contrary to our expectations for the behaviour of a single continuous structure. In the forearc, just to the east of the slab, low-velocity zones may mark the location of mantle hydration or fluid assisted melting. At longitudes east of ~70°W, along the eastern portion of the southern transect, this negative arrival could relate to the boundary between lithosphere and shallow asthenosphere. Within the centre of the southern transect, between longitudes 71.5°W and 70°W, the negative arrival appears to relate to the base of the MASH zone (Hildreth & Moorbath 1988) that feeds volcanism at shallower depths. A similar negative arrival to the one observed here is not present in the northern transect. This could in part be due to the lack of any melt present in the upper most mantle beneath the northern transect due to the cooler thermal structure resulting from the flat slab, or the slab could be pinching out the asthenosphere as has been imaged by others (e.g. Schmitz *et al.* 1999) further north in the Andes (21°S–23°S) where the slab also subducts shallowly.

Nazca slab

Within the mantle, observations that we can attribute to the presence of the subducted slab are scarce. The slab subducts at a shallow angle below the northern transect, faint arrivals indicative of a nearly horizontal interface close to 100 km depth can be seen between longitudes 70°W and 68°W (Fig. 5a). Further to the east, where we expect the slab to resume its normal dip of close to 30°, no convincing sign of the slab can be found. Similarly, below the southern transect, where the slab is also thought to be subducting at a normal angle, we do not clearly detect the slab. Some faint arrivals along the southern transect that may relate to the slab are found deepening to the east between ~70 and 130 km depths from longitudes 71°W to 69°W (Fig. 5b). Lateral averaging may contribute to the disrupted appearance of these arrivals. However, attempts to identify features related to the slab by averaging over a smaller area or inspecting individual receiver functions both provided no more evidence of the slab. Alternatively, a large amount of attenuation in the wedge between the slab and crust would hinder the propagation

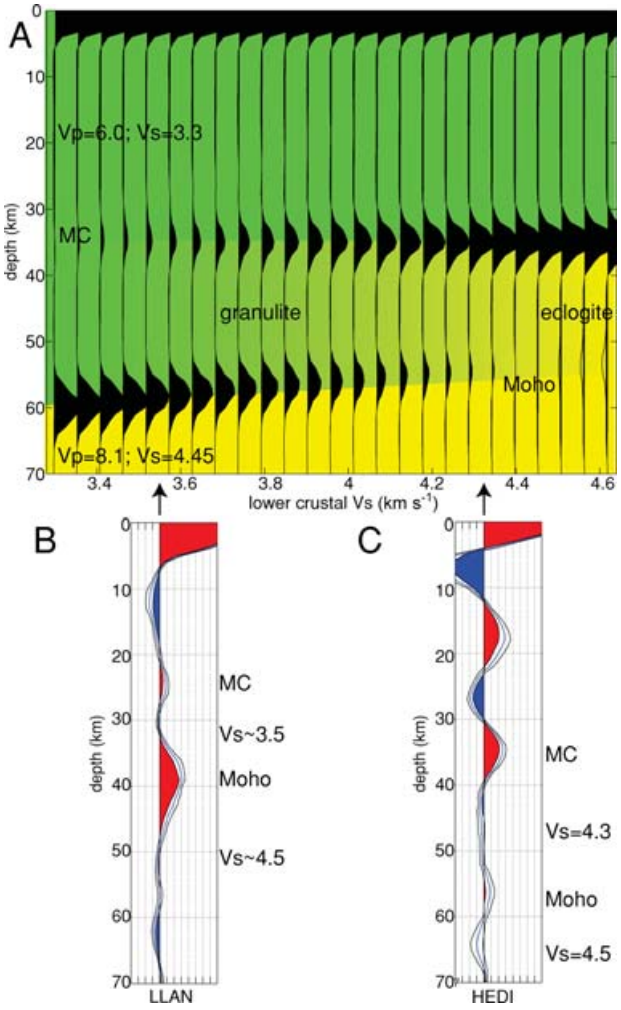

Figure 8. (a) Forward modelling results displaying synthetic receiver functions calculated from RESPKNT to illustrate the effects that the lower crustal V_S has on receiver function amplitudes. The model consisted of an upper crust with a V_S of 3.3 km s^{-1}, an upper mantle with a V_S of 4.45 km s^{-1}, and a lower crust with a V_S ranging between 3.3 km s^{-1} (left side of plot) and 4.6 km s^{-1} (right side of plot). The entire model has a constant V_P/V_S of 1.82. Mid-crustal arrivals produced by the interface between the upper and lower crust are labelled MC and increase in amplitude with increasing lower crustal V_S. The amplitude of Moho arrivals (labelled Moho) diminish in amplitude as lower crustal V_S increases. The stacked amplitude of the mid-crustal and Moho arrivals on receiver functions form LLAN (b) appear similar to synthetics with a lower crustal V_S near 3.5 km s^{-1}, while the stacked amplitudes from HEDI (c) are closer to a model with V_S of 4.3 km s^{-1}.

of *S*-wave energy. These observations differ from other studies that have clearly found subducting slabs beneath central Alaska and elsewhere in South America (e.g. Ferris *et al.* 2003; Yuan *et al.* 2000). We infer that the impedance contrast between the slab and mantle wedge in this region has been diminished causing it to be elusive to detection.

DISCUSSION

Flat slab region

Contrary to our expectations of observing a clear Moho signal and some indication of subducting lithosphere, we detect neither in central Chile and western Argentina. Previous investigations into the crustal structure of the forearc and arc region in South America identified Moho structure that deviated from expectations (e.g. Giese *et al.* 1999; Yuan *et al.* 2000) where the impedance contrast near the forearc appeared greatly reduced. The weak Moho signal observed here appears consistent with a small impedance contrast across the crust–mantle boundary resulting from high crustal velocities, low mantle velocities, or a combination of both. If the Moho were a gradient in seismic properties instead of a sharp contrast the amplitude of converted phases would be frequency dependent displaying higher amplitudes at lower frequencies. Inspection of receiver functions at a variety of frequencies to as low as 0.4 Hz all show similarly small Moho signal suggesting that a gradient Moho is unlikely to be the cause for the lack of observed Moho signal here.

We present a model of crustal and lithospheric structure that can describe many of our observations as well as the underlying mantle wedge. The lack of a clear Moho signal in the western part of our study area is a particularly curious observation. Because receiver functions are sensitive to rapid changes in seismic wave speeds, the lack of a Moho arrival could result from the diminished impedance contrast between normal crust and an especially slow mantle wedge as others have observed in regions where the mantle wedge has been serpentinized (e.g. Bostock *et al.* 2002; Brocher *et al.* 2003; Sakaguchi *et al.* 2003). Hydrated peridotite that has been converted to serpentinite will exhibit densities and seismic velocities similar to that of lower continental crust. Alternatively, the configuration of anomalously fast lower crust that approaches mantle seismic properties overlying a mantle wedge of normal mantle properties would also exhibit a small Moho signal. A mechanism that could result in crustal materials exhibiting mantle properties is the eclogitization of lower crustal material. At pressures corresponding to depths of 45–50 km, lower crustal rocks such as gabbro may be transformed to eclogite, which would possess mantle-like seismic velocities and densities (e.g. Dewey *et al.* 1993; Bousquet *et al.* 1997). We favour the hypothesis that a portion of the lower crust above the flat slab has been eclogitized. A variety of observations lead us to prefer this model. (1) The additional density of an eclogitized lower crust provides a means to isostatically balance the thick crust of the low-lying western Sierras Pampeanas. (2) Geochemical signatures of magmas erupted above the flat slab indicate contamination by garnet granultic and eclogitic material in the thickened crust (Kay & Abruzzi 1996; Kay & Mpodozis 2001, 2002). (3) The tomographic model of Wagner *et al.* (2005) above the flat slab indicates the presence of high compressional- and shear-wave speed material at the top of the mantle wedge, just below the base of the crust. This implies that we would detect an exceptionally strong Moho signal were the crust of average composition, which we do not. We note that eclogitization has only occurred within a distinct region above the flat slab, much of which is located within the boundaries of the Cuyania terrane. Thick crust is present beneath the Main Cordillera where receiver functions also exhibit a weak Moho signal. However, this observation can be explained by crust of average composition, which would balance isostatically with the high elevations of the Andes, overlying a mantle wedge that has been serpentinized, similar to that observed in the mantle forearc elsewhere in South America (Sakaguchi *et al.* 2003).

The transformation of basaltic rocks to garnet granulite and then eclogite involves the breakdown of plagioclase, addition of sodium to clinopyroxene, and the growth of garnet. The pressure and temperatures under which garnet appears has been determined experimentally and depends on the silica and magnesium content of the rocks. At pressures greater than 1.2 GPa and temperatures over

500°C eclogite is stable, the sluggish kinetics of the reaction, however, result in eclogite facies rocks not necessarily prevailing wherever such conditions exist. Instead the transformation may be suppressed after rocks enter into the eclogite stability field (Hacker 1996). Reactions involved during the transformation to eclogite require overstepping of the equilibrium conditions to overcome local free energy increases related to atomic rearrangement. The catalytic action of water during eclogitization is well known from kinetic studies of powders and rocks to significantly decrease the time needed for eclogite formation (Hacker 1996; Bjornerud & Austrheim 2004; Jackson *et al.* 2004).

The addition of water to the system greatly accelerates the transformation of rocks that are located within the pressure and temperature realm of an eclogite, but would otherwise metastably remain as granulites. However, the source of water in the region of the Argentinean flat slab remains enigmatic. It appears the water source responsible for producing the wide-scale eclogitization of the crust must have been a transient phenomenon in this setting. There is no evidence for steady-state hydration of the mantle wedge as inferred from high shear wave-speeds (Wagner *et al.* 2005) and the lack of recent magmatism that would be expected to overlie a hydrated wedge. Possible factors that could be responsible for transient water transportation include a period of subduction erosion and the release of water from subducted sediments accumulated along the flanks of the already subducted Juan Fernandez ridge. Alternatively, the source of water may have been within the terrane itself, removing the need for water transport into the lower crust. The lower crust of the Cuyania terrane would readily transform to eclogite once thickened to greater pressures if it already contained the necessary water in hydrous minerals to serve as a catalyst. The tectonic history of this region is therefore particularly important to the development of the present crustal structure.

Highlights of past events that proceeded, and are responsible for, the current crustal structure are summarized below and are based on tectonic histories presented by Yañez *et al.* (2001), Kay & Mpodozis (2002) and Ramos *et al.* (2002). Starting in the Early Miocene (27–20 Ma) the crust had not yet thickened, evidence that the region still possessed normal to slightly thickened crust is inferred from trace element patterns of magmatism within the Doña Ina group that indicate equilibrium with pyroxene and amphibole bearing rocks. The Máquinas basalts (Fig. 1) erupted from volcanoes during this time in the backarc east of El Indio possess interplate REE ratios, and are indicative of an eruption in an extensional backarc environment over a steeply dipping slab. Compositional differences within the Doña Ana volcanic field (Fig. 1) denote a period of deformation near 20 Ma. Rocks that comprise the Tilito formation, which erupted from 27 to 23 Ma, mostly consisted of silicic and rhyodacitic materials. In contrast, mafic and basaltic rocks comprise the younger Escabroso formation that erupted between 21 and 18 Ma. The transition away from a garnet-poor gabbroic residue that was equilibrated at depths of less than 40 km in the Early Miocene for the Main Cordillera to a garnet-bearing granulitic or eclogitic residue in the later Miocene that was equilibrated at depth of greater than 50 km is supported by trace-element modelling and indicative of crustal thickening (Kay *et al.* 1991; Kay & Abruzzi 1996). The crust in this region thickened from close to 40 km at 20 Ma to its present thickness of over 60 km by 6 Ma (Kay & Abruzzi 1996). Most crustal thickening resulted from shortening associated with thrusting along thin-skinned thrust faults above a decollement in the Precordillera and thick-skinned block faults in the Sierras Pampeanas. The base of the crust would have entered into the eclogite stability field while reaching depths greater than ∼45 km.

Changes in convergence parameters between the South American and Nazca plates due to the breakup of the Farallon plate into the Nazca and Cocos plates (Ramos *et al.* 2002) ushered in the present period of orthogonal convergence (Cande & Leslie 1986) and may be responsible for the compressive forces during the Miocene. A period of plate motion reorganization from oblique to more orthogonal convergence in the Early Miocene provides conditions conducive of subduction erosion (Jordan *et al.* 2001) and could have facilitated the transportation of water into the mantle.

The latest Early Miocene (20–16 Ma), can be characterized as a transitional period from an extensional to compressional tectonic regime in the flat slab region marked by magmatic lulls in some regions and the eastward migration of the arc in the south and broadening of the arc elsewhere. Initial shallowing of the slab occurred during this period as indicated by eastward broadening of the arc, high angle thrusting in the Main Cordillera, the termination of mafic backarc volcanism, and the inception of deformation in the Precordillera. The distinctive transient patterns of REE ratios, indicative of high pressure mineral residuals in early flat-slab magmas, are difficult to explain using a model of lower crustal contamination such as the MASH model (Hildreth & Moorbath 1988) because it would require unreasonable variations in crustal thickness over a short period of time (Kay & Mpodozis 2002). Instead the transport of tectonically removed continental crust from the forearc into the mantle source region above the slab could produce the changes in REE patterns (Kay & Mpodozis 2002) by processes associated with forearc subduction erosion (von Huene & Scholl 1991; Stern 1991; Kay *et al.* 1999) and provide a source of water needed for the eclogitization of the lower crust.

Still, the pathways and mechanisms by which fluids traversed from mantle wedge into crust remain unknown. Ascent paths of fluids and melts as inferred from regions of high *P*-wave attenuation have been found to be complex, exhibiting a significant amount of variability over a small area (Schurr *et al.* 2003). Two interrelated mechanisms for fluid transport in the mantle wedge up into the crust are porous flow along grain boundaries and buoyancy-driven propagation of fluid filled cracks or fractures. Fluid overpressure leads to weakening and embrittlement resulting in the transition from separate pores to interconnected cracks (Miller *et al.* 2003). The migration of fluids via porous flow is slow, but extensively affects the material through which it transects, conversely fluids travel much more quickly through cracks, resulting in large fluid fluxes along limited flow paths (Miller *et al.* 2003). The images of a region nearly 300 km in extent that we propose has undergone eclogitization suggesting the presence of wide-spread fluids, but it would have had to occur since the time when the slab began flattening between 20 and ∼12 Ma. Whether the source of water even originated from the wedge or was originally present within the Cuyania terrane cannot be determined here.

Lower crustal eclogitization

In order to test the effects of lower crustal shear-wave speeds on receiver function amplitudes, we present forward modelling results for models with a range of lower crustal velocities (Fig. 8a) utilizing the waveform forward modelling code RESPKNT (Randall 1994). We use this approach to calculate synthetic seismograms for a three layered model comprised of an upper crust with a V_P of 6.0 km s^{-1} and V_S of 3.3 km s^{-1}, a mantle with a V_P of 8.1 km s^{-1} and V_S of 4.45 km s^{-1}, and a lower crust with a variable V_P between 6.0 km s^{-1} and 8.4 and *S*-wave velocities that are proportional to the *P*-wave velocities using a constant V_P/V_S of 1.82, which approximates the

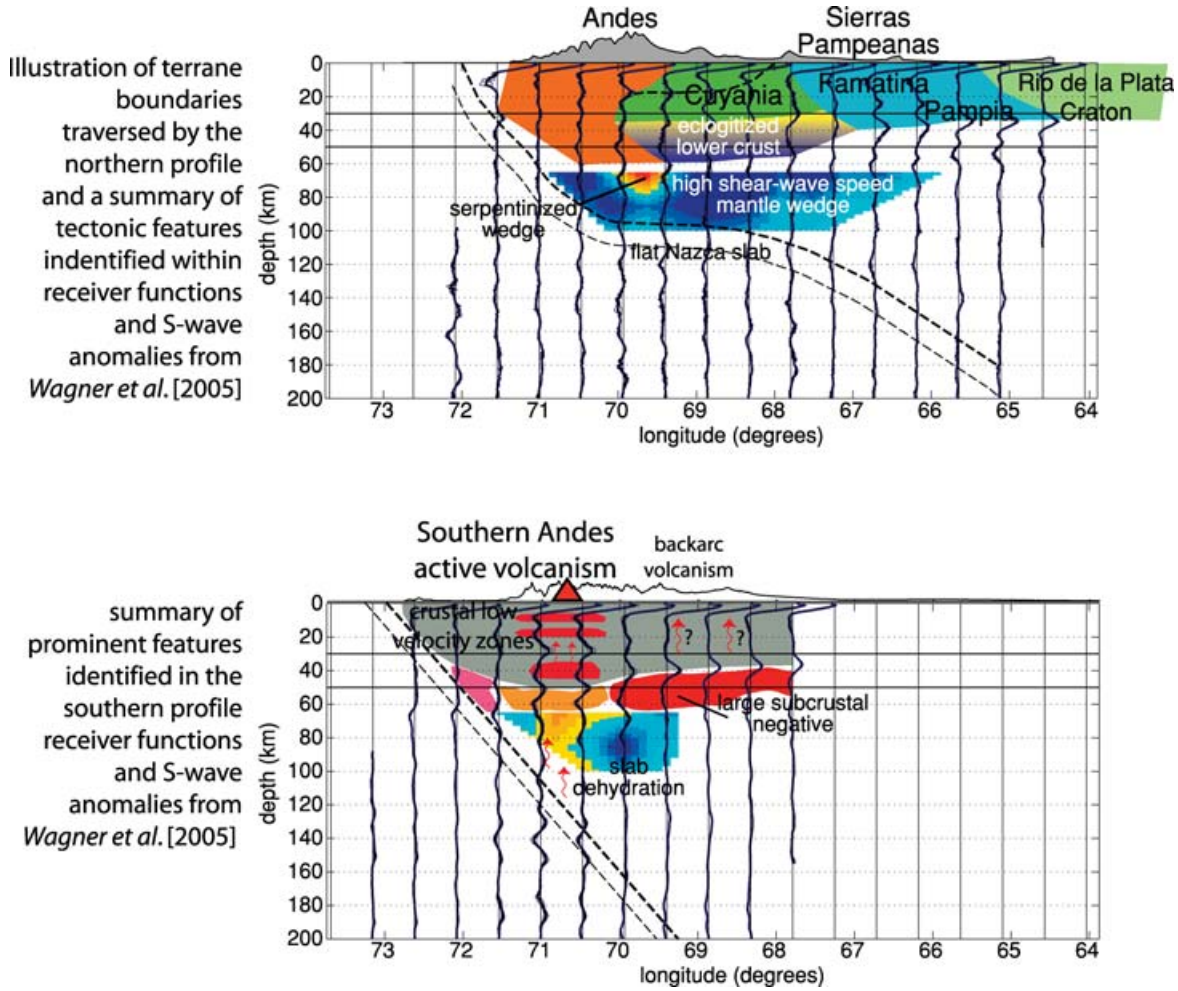

Figure 9. Summary cartoon of northern and southern transects presenting major observations of CHARGE receiver functions. Variations in the Moho signature in the northern transect correlate well with locations of terrane boundaries. Large negative arrivals within the crust coincide with a region of active volcanism within the southern transect. Multiple factors may be responsible for a subcrustal negative arrival in the southern transect; mantle hydration or melting of subducted material could be at play in the west (pink), further east the base of the MASH zone could produce the negative (orange), the base of the lithosphere could produce the negative found to the east (red). Nearby cross-sections from a local shear-wave tomographic model (Wagner *et al.* 2005) are also presented for the northern and southern cross-sections (high (blue) and low (red) speed anomalies range between +4 per cent and −4 per cent).

average crust beneath the western Sierras Pampeanas. The value for V_P of 8.1 km s^{-1} for the mantle comes from the *Pn* analysis of crustal structure along the northern transect of the CHARGE array (Fromm *et al.* 2004).

Forward modelling results illustrate that models with a slow lower crust (lower crustal V_P of 6.4 km s^{-1} and $V_S \sim 3.5$ km s^{-1}) appear similar to observations from LLAN (Fig. 8b). Receiver functions from the station HEDI exemplify the complex signal from other stations within the western Sierras Pampeanas. The arrival from the Moho at HEDI is much smaller than that at LLAN (Fig. 8c). Additional arrivals are also present at each of the stations in the western Sierras Pampeans that we attribute to the presence of a boundary between the upper and lower crust. The mid-crustal arrival is very small at LLAN, which is consistent with models that possess a very small velocity change within the crust. In contrast, HEDI displays a much larger mid-crustal arrival, which in fact is larger than the Moho arrival there. This pattern of arrivals is similar to models with a significantly faster lower crust than upper crust (lower crustal V_P of 7.8 km s^{-1} and $V_S \sim 4.3$ km s^{-1}). For comparison, this lower crustal compressional wave velocity is greater than the high lower crustal V_P of 7.3 km s^{-1} within a local model for this region developed to locate aftershocks near the Sierra Pie de Palo (Bollinger & Langer 1988). Our observations and modelling results indicate the need for a larger lower crustal V_P because synthetic receiver functions calculated for models with a smaller V_P (and correspondingly lower V_S) possess a much larger Moho signal than that observed for HEDI.

In order to gain insight into the petrologic conditions that could produce a lower crustal V_P and V_S in this range we calculate the seismic properties of rocks within this pressure and temperature range. Using mineralogical compositions of garnet, clinopyroxene, and plagioclase from an arc environment (Ducea & Saleeby 1996), we calculate seismic properties for granulites and eclogites by employing the program developed by Hacker *et al.* (2003). For a granulite composed of 65 per cent plagioclase, 15 per cent garnet, and 20 per cent clinopyroxene by volume, we calculate a V_S and density of 3.9 km s^{-1} and 3.0 g cm^{-3} at 1.5 GPa and 500°C. Both the density and velocity increase by increasing the garnet content at the expense

of plagioclase as the composition trends from a granulitic composition to a garnet granulite. Whereas an eclogite composed of 50 per cent garnet and 50 per cent clinopyroxene by volume will have a V_S of 4.6 km s^{-1} and a density of 3.6 g cm^{-3} under the same conditions. Although these values do not reflect the exact composition of the South American lower crust, they clearly illustrate the high seismic velocities attainable by lower crustal rocks composed of eclogite, and the differences in velocity and density between granulite and eclogite.

Based on the velocities calculated above it does not appear that the whole lower crust has been eclogitized because the velocity of eclogite alone is too high with respect to the observed *Pn* velocities to produce the observed Moho signal. Additional evidence against the complete eclogitization of the lower crust comes from density considerations and attempts to isostatically balance crustal columns within the eastern and western Sierras Pampeanas. Structural models of a homogeneous crust with a density 400 kg/m^3 less than the mantle derived from gravimetric observations of negative Bouguer anomalies have indicated the need for thin crust of $\sim$ 40 km thick across much of the flat slab region at 30°S (Introcaso *et al.* 1992). This model produced thinner crust than seismic investigations above the flat slab that found crustal thicknesses of over 50 km (e.g. Regnier *et al.* 1994). This discrepancy motivated later gravity analysis to consider the contribution of the subducted Nazca slab in their models. Leaving crustal densities constant and assuming an additional density contribution from the slab would lead to crustal models that are $\sim$10 km thicker and still satisfy the observed Bouguer anomaly (Gimenez *et al.* 2000) thus reconciling differences between seismic and gravity analysis.

Still, a remaining inconsistency within this line of reasoning relates to the attribution of additional density to a flat slab, presumably the reduction of subduction angle would accommodate a reduction in the density difference between the slab and mantle. A possible internally consistent alternative model that can satisfy both seismic observations of thicker crust and gravity constraints for a thin low-density layer would be to allow crustal densities to vary, thus transferring the needed additional dense material away from the slab and placing it into the crust. Our observations, suggestive of a lower crust that has been eclogitized to some degree, indicate that such a scenario may be present in the western Sierras Pampeanas where a normal density upper crust of $\sim$30 km thick is underlain by a dense lower crust resulting in a total crustal thickness over 50 km that matches gravity observations without the need of a dense slab.

Southern Volcanic Zone

The southern CHARGE transect crosses the Andes near volcanic centres that may be underlain by the MASH zone (Hildreth & Moorbath 1988) where mantle material enters into the crust promoting crustal melt and eventually leading to volcanism. Water released from the slab causes partial melting of the overlying mantle and initiates the formation of the volcanic arc. As magmas pass through the continental crust, they further differentiate and assimilate crust (e.g. Hildreth & Moorbath 1988). The nature of this phenomenon, involving partially molten mantle material within partially molten crust blurs the boundary between the crust and mantle, which could be responsible for reducing the observed Moho signal in the Main Cordillera of the Southern transect. The general structure of the plumbing system underlying the Southern Volcanic Zone can be partially identified in the crustal structure of the southern transect.

The origin of basaltic to dacitic volcanic rocks present in the Southern Volcanic Zone is important because the region contains a wide compositional range of lavas. Differences in the compositions and petrography of the mafic lavas and inclusions and the extent to which they have interacted with crustal melts may be explained by the generation of a silicic magmatic system in a region characterized by repeated basaltic injections (e.g. Feeley *et al.* 1998). The petrogenic process of producing andesitic and dacitic lavas of the Southern Volcanic Zones includes assimilation of garnet-bearing, possibly mafic lower continental crust by mantle derived basaltic magmas, as well as intrusion of basaltic andesitic magmas into shallow reservoirs containing crystal-rich dacitic magmas and their subsequent mixing to produce hybrid basaltic andesitic and andesitic magmas. Major element, trace element, and Sr-isotopic data for the volcanic rocks within the Southern Volcanic field provide evidence for shallow silicic reservoirs within a region distinguished by warm crustal temperatures resulting from basaltic activity and high magma supply rates (Feeley *et al.* 1998). Detailed petrographic and compositional study of two groups of gabbroic xenoliths from the Tatara-San Pedro Complex in the Southern Volcanic Zone (Fig. 1) indicates multistage crystallization histories involving migration and melts and aqueous fluids through the crust (Costa *et al.* 2002).

The crustal structure observed along the southern transect indicates the presence of multiple low-velocity zones within the mid- and lower-crust and is consistent with petrologic models of andesitic and dacitic petrogenesis. The lower of these two low-velocity zones is near 40 km depth and may indicate the region where basaltic material intrudes into the lower crust. A magma chamber at this depth range may assimilate garnet and mafic material from the lower crust. At shallower levels within the crust, between 10 and 20 km depth, low-velocity zones may mark the location of a reservoir of silicic magma.

The large coherent negative arrival beneath the crust at this latitude appears to mark the location of low-velocity material in the mantle that feeds the shallower crustal magma chambers. The continuation of this negative arrival in the mantle well to the east of the crustal negative arrivals may in part be responsible for the extensive Quaternary basaltic and andesitic backarc volcanism in the Southern Volcanic Zone (Fig. 1) (Jordan *et al.* 1983). Corner flow within the mantle wedge at this latitude drawing in asthenospheric material offers a possible explanation for the backarc volcanism and associated large negative arrival in the upper mantle at this latitude.

CONCLUSIONS

A summary of our findings is presented in Fig. 9. Within the northern transect we identify variations in crustal thickness and in the signature of the Moho that correlate with the location of terrane boundaries. In agreement with a previous *Pn* investigation (Fromm *et al.* 2004), crustal thickness increases from east to west, obtaining its maximum thickness of 63 km beneath the high Andes near a longitude 70°W. Crust of increased thickness (>50 km) is not geographically limited to the location of the high Andes, extending instead into the western Sierras Pampeanas, within the backarc, where surface elevations are significantly lower. A possible explanation that can reconcile the presence of thick crust with low surface elevations is that the lower crust has been partially eclogitized making it denser than average crust thus preventing it from isostatically rising. The lack of a strong Moho signal in the western Sierras Pampeanas, indicative of a small impedance contrast, can also be explained by eclogitic lower crust, which has *S*-wave speeds closer to that of the mantle, which have been reported to be particularly high in this region (Wagner *et al.* 2005) (Fig. 9). Mid-crustal arrivals

can be clearly found in the central portion of the northern transect that mark the upper boundary of eclogitized lower crust near 35 km depth and the location of a decollement that accommodated thrusting at 20 km (Fig. 9).

The Moho signal is also complicated in the western portion of the southern transect where crustal low-velocity zones are located within the MASH zone. These arrivals occur above a region of low shear-wave speeds in the mantle wedge (Wagner *et al.* 2005) (Fig. 9) possibly highlighting the path taken by melt and fluids from the slab, through the wedge, into the crust and finally erupted out of the volcanoes of the Southern Volcanic Zone. The entire length of crust sampled by the southern transect possesses a high V_P/V_S value (Fig. 7) which can result from the presence of fluids or magma within the crust, just as would be predicted for a region with extensive volcanism.

We expected to find a strong receiver function arrival indicative of a significant velocity contrast between the subducted Nazca slab and mantle. The lack of any such arrival could indicate that no such velocity contrast exists in this location. Small arrivals are found near the expected location of the slab, as inferred from the location of seismicity, but they are not large enough for us to be confident that they do indeed mark the location of the slab. Comparing the location of slab seismicity to our crustal structure we find that the region of thickened eclogitized crust appears to be limited to the region where the slab subducts at a shallow angle. This correlation may imply that factors related to the flat slab contributed to the eclogitized lower crust, but the influence of the slab on the crust currently remains unresolved and warrants further investigation and motivates improved models of crustal and upper most mantle velocities.

ACKNOWLEDGMENTS

Our work benefited from the *Pn* analysis performed by Robert Fromm and is dedicated to his memory. We might not have been able to find the Moho without him. We are grateful for the work done by Todd Shearer helping initiate this study by beginning to calculate receiver functions from the CHARGE array. The National Science Foundation supported this research under grant EAR9811870. We acknowledge INPRES, the National University of San Juan (Argentina), and the University of Chile for their logistical support and assistance in the field and thank the entire CHARGE Working Group for their many efforts and contributions to this work. The instruments used in the CHARGE field experiment were provided by the PASSCAL facility of the Incorporated Research Institutions for Seismology (IRIS) through the PASSCAL Instrument Center. The collected data are available through the IRIS Data Management Center. The National Science Foundation under Cooperative Agreement EAR-0004370 supports the facilities of the IRIS Consortium.

REFERENCES

Allmendinger, R.W., Ramos, V.A., Jordan, T.E., Palma, M. & Isacks, B.L., 1983. Paleogeography and Andean structural geometry, northwest Argentina, *Tectonics,* **2,** 1–16.

Allmendinger, R.W., Figueroa, D., Snyder, D., Beer, J., Mpodozis, C. & Isacks, B.L., 1990. Foreland shortening and crustal balancing in the Andes at 30°S latitude, *Tectonics,* **9,** 789–809.

Alvarado, P., Beck, S., Zandt, G., Araujo, M. & Triep, E., 2005. Crustal deformation in the south-central Andes back-arc terranes as viewed from regional broadband seismic waveform modelling, *Geophys. J. Int.,* **163,** 580–598.

Astini, R.A. & Thomas, W.A., 1999. Origin and evolution of the Precordillera terrane of western Argentinia: a drifted Laurentian orpan, in *Laurenti-Gondwana Connections before Pangea*, eds Ramos, V.A. & Keppie, J.D., Boulder, Colorado, Geological Society of America Special Paper 336.

Bird, P., 1984. Laramide crustal thickening event in the Rocky Mountain foreland and Great Plains, *Tectonics,* **3,** 741–758.

Bjornerud, M.G. & Austrheim, H., 2004. Inhibited eclogite formation: the key to the rapid growth of strong and buoyant Archean continental crust, *Geology,* **32,** 765–768.

Bollinger, G.A. & Langer, C.J., 1988. Development of a velocity model for locating aftershocks in the Sierra Pie de Palo region of western Argentina, *US. Geol. Surv. Bull.,* 1795.

Bostock, M.G., Hyndman, R.D., Rondenay, S. & Peacock, S.M., 2002. An inverted continental Moho and serpentization of the forearc mantle, *Nature*, **417,** 536–538.

Bousquet, R., Goffe, B., Henry, H., Le Pichon, X. & Chopin, C., 1997. Kinematic, thermal and petrological model of the Central Alps: Lepontine metamorphism in the upper crust and eclogitisation of the lower crust, *Tectonophysics,* **273,** 105–127.

Brocher, T.M., Parsons, T., Trehu, A.M., Snelson, C.M. & Fisher, M.A., 2003. Seismic evidence for widespread serpentinized forearc upper mantle along the Cascadia margin, *Geology,* **31,** 267–270.

Cahill, T. & Isacks, B.L., 1992. Seismicity and the shape of the subducted Nazca plate, *J. geophys. Res.,* **97,** 17 503–17 529.

Cande, S.C. & Leslie, R.B., 1986. Late Cenozoic tectonic s of the southern Chile trench, *J. geophys. Res.,* **91,** 471–496.

Clouser, R.H. & Langston, C.A., 1995. Effect of sinusoidal interfaces on teleseismic P-wave receiver functions, *Geophys. J. Int.,* **123,** 541–558.

Costa, F., Dungan, M.A. & Singer, B.S., 2002. Hornblende- and phlogopite-bearing gabbroic xenoliths from volcan San Pedro (36°S), Chilean Andes: evidence for melt and fluid migration and reaction in subduction-related plutons, *J. Petrol,* **43,** 219–241.

Dewey, J.F., Ryan, P.D. & Andersen, T.B., 1993. Orogenic uplift and collapse, crustal thickness, fabrics and metamorphic phase changes, the role of eclogites, in *Magmatic Processes and Plate Tectonics*, Vol. 76, pp. 3–38, eds Prichard, H.M., Alabaster, T., Harris, N.B.W. & Neary, C.R., Geological Society, Special Publication.

Ducea, M.N. & Saleeby, J.B., 1996. Buoyancy sources for a large, unrooted mountain range, the Sierra Nevada, California: Evidence from xenolith thermobarometry, *J. geophys. Res.,* **101,** 10 029–10 041.

Dueker, K.G. & Sheehan, A.F., 1997. Mantle discontinuity structure from mid-point stacks of converted P to S waves across the Yellowstone hotspot track, *J. geophys. Res.,* **102,** 8313–8327.

Engdahl, E.R., van der Hilst, R.D. & Buland, R.P., 1998. Global teleseismic earthquake relocation with improved travel times and procedures for depth determination, *Bull. seism. Soc. Am.,* **88,** 722–743.

Feeley, T.C., Dungan, M.A. & Frey, F.A., 1998. Geochemical constraints on the origin of mafic and silicic magmas at Cordon El Guadal, Tatara-San Pedro Complex, central Chile, *Contrib. Mineral. Petrol.,* **131,** 393–411.

Ferris, A., Abers, G.A., Christensen, D.H. & Veenstra, E., 2003. High resolution image of the subducted Pacific (?) plate beneath central Alaska, 50–150 km depth, *Earth planet. Sci. Lett.,* **214,** 575–588.

Flueh, E.R. *et al.,* 1998. Seismic investigation of the continental margin off- and onshore Valparaiso, Chile, *Tectonophysics,* **288,** 251–263.

Fromm, R., Zandt, G. & Beck, S.L., 2004. Crustal thickness beneath the Andes and Sierras Pampeanas at 30°S inferred from Pn apparent phase velocities, *Geophys. Res. Lett.,* **31,** doi:10.1029/2003GL019231.

Giese, P., Scheuber, E., Schilling, F., Schmitz, M. & Wigger, P., 1999. Crustal thickening processes in the Central Andes and the different natures of the Moho-discontinuity, *J. South Am. Earth Sci.,* **12,** 201–220.

Gilbert, H.J. & Sheehan, A.F., 2004. Images of crustal variations in the intermountain west, *J. geophys. Res.,* **109,** B03306, doi:10.1029/2003JB002730.

Gimenez, M.E., Martinez, M.P. & Introcaso, A., 2000. A gravity model based mainly on gravity data in the area between the Bermejo Basin and the Sierras de Valle Fertil, Argentina, *J. South Am. Earth Sci.,* **13,** 275–286.

Grier, M.E., Salfity, J.A. & Allmendinger, R.W., 1992. Andean reactivation of the Cretaceous Salta rift, northwestern Argentina, *J. South Am. Earth Sci.,* 351–371.

Gutscher, M., Spakman, W., Bijwaard, H. & Engdahl, E., 2000. Geodynamics of flat subduction: Seismicity and tomographic constraints from the Andean margin, *Tectonics,* **19,** 814–833.

Hacker, B.R., 1996. Eclogite formation and the rheology, buoyancy, seismicity, and H_2O content of oceanic crust, in *Subduction top to bottom*, pp. 337–246, eds Bebout, G.E., Scholl, D.W., Kirby, S.H. & Platt, J.P., AGU, Washington, DC.

Hacker, B., Abers, G. & Peacock, S., 2003. Subduction factory 1. Theoretical mineralogies, densities, seismic wave speeds, and H_2O contents, *J. geophys. Res.,* **108,** 2029, doi:10.1029/2001JB001127.

Hildreth, W. & Moorbath, S., 1988. Crustal contributions to arc magmatism in the Andes of central Chile, *Contrib. Mineral. Petrol.,* **98,** 455–489.

Introcaso, A., Pacino, M.C. & Fraga, H., 1992. Gravity, isostasy and Andean crustal shortening between latitudes 30 and 35°S, *Tectonophysics,* **205,** 31–48.

Jackson, J.A., Austrheim, H., McKenzie, D. & Priestley, K., 2004. Metastability, mechanical strength, and the support of mountain belts, *Geology,* **32,** 625–628.

Jarrard, R.D., 1986. Relations among subduction parameters, *Rev. Geophys.,* **24,** 217–284.

Jordan, T.E., Isacks, B.L., Allmendinger, R.W., Brewer, J.A., Ramos, V.A. & Ando, C.J., 1983. Andean tectonics related to the geometry of the subducted Nazca Plate, *Geol. soc. Am. Bull.,* **94,** 341–361.

Jordan, T.E., Burns, W.M., Veiga, R., Pangaro, F., Copeland, P., Kelley, S. & Mpodozis, C., 2001. Extension and basin formation in the southern Andes caused by increased convergence rate: a mid-Cenozoic trigger for the Andes, *Tectonics,* **20,** 308–324.

Kay, S.M. & Abruzzi, J.M., 1996. Magmatic evidence for Neogene lithospheric evolution of the central Andean flat-slab between 30°S and 32°S, *Tectonphysics,* **259,** 15–29.

Kay, S.M. & Mpodozis, C., 2001. Central Andean Ore Deposits Linked to Evolving Shallow Subduction Systems and Thickening Crust, *GSA Today,* **11,** 4–9.

Kay, S.M. & Mpodozis, C., 2002. Magmatism as a probe to the Neogene shallowing of the Nazca plate beneath the modern Chilean flat-slab, *J. South Am. Earth Sci.,* **15,** 39–57.

Kay, S.M., Maksaev, V., Mpodozis, C., Moscoso, R. & Nasi, C., 1987. Probing the evolving Andean lithosphere: middle to late Tertiary magmatic rocks in Chile over the modem zone of subhorizontal subduction (29–31.5°S), *J. geophys. Res.,* **92,** 6173–6189.

Kay, S.M., Maksaev, V., Mpodozis, C., Moscoso, R., Nasi, C. & Gordillo, C.E., 1988. Tertiary Andean magmatism in Argentina and Chile between 28–33°S: Correlation of magmatic chemistry with a changing Benioff zone, *J. South Am. Earth Sci.,* **1,** 21–38.

Kay, S.M., Mpodozis, C., Ramos, V.A. & Munizaga, F., 1991. Magma source variations for mid-late Tertiary magmatic rocks associated with a shallowing subduction zone and a thickening crust in the central Andes (28° to 33°S), in *Andean Magmatism and its Tectonic Setting*, Vol. 265, pp. 113–137, eds Harmon, R.S. & Rapela, C.W., Geological Society of America Special Paper.

Kay, S.M., Mpodozis, C. & Coira, B., 1999. Magmatism, tectonism, and mineral deposits of the Central Andes (22°–33°S latitude), in *Geology and Ore Deposits in the Central Andes*, Vol. 7, pp. 27–59, ed. Skinner, B., Society of Economic Geology Special Publication.

Langston, C.A., 1977. The effect of planar dipping structure on source and receiver response for constant ray parameter, *Bull. seism. Soc. Am.,* **67,** 1029–1050.

Li, A., Fischer, K.M., Wysession, M.E. & Clarke, T.J., 1998. Mantle discontinuities and temperature under the North American continental keel, *Nature,* **395,** 160–163.

Ligorria, J.P. & Ammon, C.J., 1999. Iterative deconvolution and receiver function estimation, *Bull. seism. Soc. Am.,* **89,** 1395–1400.

Miller, S.A., van der Zee, W., Olgaard, D.L. & Connolly, J.A.D., 2003. A fluid-pressure feedback model of dehydration reactions: experiments, modeling, and application to subduction zones, *Tectonophysics,* **370,** 241–251.

Owens, T.J., Zandt, G. & Taylor, S.R., 1984. Seismic evidence for an ancient rift beneath the Cumberland Plateau, Tennessee: a detailed analysis of broadband teleseismic P waveforms, *J. geophys. Res.,* **89,** 7783–7795.

Owens, T.J., Crosson, R.S. & Hendrickson, M.A., 1988. Constraints on the subduction geometry beneath western Washington from broadband teleseismic waveform modeling, *Bull. seism. Soc. Am.,* **73,** 1319–1334.

Phinney, R.A., 1964. Structure of the Earth's crust from spectral behavior of long-period waves, *J. geophys. Res.,* **69,** 2997–3017.

Ramos, V.A., Cegarra, M. & Cristallini, E., 1996. Cenozoic tectonics of the high Andes of west-central Argentina (30–36°S latitude), *Tectonophysics,* **256,** 185–200.

Ramos, V.A., Cristallini, E.O. & Perez, D.J., 2002. The Pampean flat-slab of the Central Andes, *J. South Am. Earth Sci.,* **15,** 59–78.

Randall, G.E., 1994. Efficient calculation of complete differential seismograms for laterally homogeneous earth models, *Geophys. J. Int.,* **118,** 245–254.

Regnier, M., Chiu, J.M., Smalley, R., Jr, Isacks, B.L. & Araujo, M., 1994. Crustal thickness variation in the Andean foreland, Argentina, from converted waves, *Bull. seism. Soc. Am.,* **84,** 1097–1111.

Sakaguchi, K., Gilbert, H., Zandt, G., Beck, S. & the CHARGE working group, 2003. An investigation into crustal structure of South America; the continent that is missing some of its Moho, *EOS, Trans. Am. geophys. Un.,* **84,** Fall Meet. Suppl., Abstract S41D.

Schmidt, C.J., Astini, R.A., Costa, C.H., Gardini, C.E. & Kraemer, P.E., 1994. Cretaceous rifting, alluvial fan sedimentation, and Neogene inversion, southern Sierras Pampeanas, Argentina, in *Petroleum Basins of South America*, Vol. 62, pp. 341–358, eds Tankard, A., Suarez, R., Helsink, H.J., American Association of Petroleum Geologists, Memoir.

Schmitz *et al.,* 1999. The crustal structure beneath the Central Andean forearc and magmatic arc as derived from seismic studies—the PISCO 94 experiment in northern Chile (21°–23°S), *J. South Am. Earth Sci.,* **12,** 237–260.

Schurr, B., Asch, G., Rietbrock, A., Trumbull, R. & Haberland, C., 2003. Complex patterns of fluid and melt transport in the central Andean subduction zone revealed by attenuation tomography, *Earth planet. Sci. Lett.,* **215,** 105–119.

Stern, C.R., 1991. Role of subduction erosion in the generation of Andean magmas, *Geology,* **19,** 79–81.

van Hunen, J., van den Berg, A.P. & Vlaar, N.J., 2002. On the role of subducting oceanic plateaus in the development of shallow flat subduction, *Tectonophysics,* **352,** 317–333.

von Huene, R. & Scholl, D.W., 1991. Observations at convergent margins concerning subduction, subduction erosion and growth of continental crust, *Rev. Geophys.,* **29,** 279–316.

Wagner, L.S., Beck, S.L. & Zandt, G., 2005. Upper mantle structure in the south central Chilean subduction zone (30 to 36S), *J. geophys. Res.,* doi:10.1029/2004JB003238.

Whitman, D., Isacks, B.L., Chatelain, J.-L., Chiu, J.-M. & Perez, A., 1992. Attenuation of high frequency seismic waves beneath the central Andean plateau, *J. geophys, Res.,* **97,** 19 929–19 947.

Wilson, C.K., Jones, C.H. & Gilbert, H.J., 2003. Single-chamber silicic magma system inferred from shear wave discontinuities of the crust and uppermost mantle, Coso geothermal area, California, *J. geophys. Res.,* **108,** 2226, doi:10.1029/2002JB001798.

Yañez, G.A., Ranero, C.R., von Huene, R. & Diaz, J., 2001. Magnetic anomaly interpretation across the southern central Andes (32°–34°S): the role of the Juan Fernandez ridge in the late Tertiary evolution of the margin, *J. geophys. Res.,* **106,** 6325–6345.

Yañez, G., Cembrano, J., Pardo, M., Ranero, C. & Selles, D., 2002. The Challenger-Juan Fernandez-Maipo major tectonic transition of the Nazca-Andean subduction system at 33–34°S: geodynamic evidence and implications, *J. South Am. Earth Sci.,* **15,** 23–38.

Yuan *et al.,* 2000. Subduction and collision processes in the Central Andes constrained by converted seismic phases, *Nature,* **408,** 958–961.

Zandt, G., Myers, S.C. & Wallace, T.C., 1995. Crust and mantle structure across the Basin and Range-Colorado Plateau boundary at 37 N latitude and implications for Cenozoic extensional mechanism, *J. geophys. Res.,* **100,** 10 529–10 548.

Zandt, G., Gilbert, H., Owens, T.J., Ducea, M., Saleeby, J. & Jones, C.H., 2004. Active foundering of a continental arc root beneath the southern Sierra Nevada in California, *Nature,* **431,** 41–46.

Zapata, T.R. & Allmendinger, R.W., 1996. Thrust front zone of the Precordillera, Argentina: a thick skinned triangle zone, *AAPG Bulletin,* **80,** 359–381.